Pergamon

Deep-Sea Research II, Vol. 43, No. 7–8, pp. 1947–1970, 1996

PII: S0967-0645(96)00051-3
0967-0645/96 $15.00 + 0.00

Rapid visualization of plankton abundance and taxonomic composition using the Video Plankton Recorder

CABELL S. DAVIS,* SCOTT M. GALLAGER,* MARTIN MARRA† and W. KENNETH STEWART†

(*Received* 6 *January* 1995; *in revised form* 29 *November* 1995; *accepted* 5 *May* 1996)

Abstract—Traditional methods for determining spatial distributions of planktonic taxa involve net, pump, and bottle collections followed by the tedious and time-consuming task of plankton sample analysis. Thus, plankton ecologists often require months or even years to process samples from a single study. In this paper, we present a method that allows rapid visualization of the distribution of planktonic taxa while at sea. Rapid characterization of plankton distributions is essential in the dynamic physical environment, where biological and physical patterns can change quickly. Such a "sample-and-observe" capability is necessary for mapping ephemeral features (such as patches, eddies, jets, plumes) and determining appropriate locations to conduct more localized sampling, including *in situ* observational studies. We describe the techniques used in imaging the plankton, analyzing the video, and visualizing the data. We present an example of at-sea data analysis conducted aboard R.V. *Columbus Iselin* on Georges Bank in May 1994 and visualizations of the 3-dimensional distribution of selected planktonic taxa in a 2 × 2 km × 90 m volume of seawater. A video of the image processing and visualization is included on the CD-ROM accompanying this volume and is an essential part of this paper. Copyright © 1996 Elsevier Science Ltd

INTRODUCTION

Understanding the processes controlling abundance of marine plankton species in time and space is a fundamental goal of Biological Oceanography. Current knowledge of distributions of planktonic taxa in the ocean is based on data from point samples collected by nets, bottles, and pumps, whereas plankton population dynamics are affected over a continuum of scales from microns to kilometers (Marine Zooplankton Colloquium, 1989; Davis *et al.*, 1991; Denman and Gargett, 1995). In addition, because of the time-consuming nature of plankton sample analysis, plankton ecologists often require months or even years to complete analysis of samples from a single study.

The advent of acoustic, electronic, and non-imaging optical plankton samplers has enabled rapid collection of continuous distributional information of particle size composition in the ocean (Sheldon *et al.*, 1972; Denman and Mackas, 1977; Herman, 1988; Holliday *et al.*, 1989; GLOBEC, 1993). Such data have led to the establishment and testing of important theories on the dynamics controlling particle size structure in the ocean (e.g. Sheldon *et al.*, 1977; Platt and Denman, 1978; Sprules and Munawar, 1986). By augmenting such measurements with concurrent plankton net hauls, insights have been

* Department of Biology, Woods Hole Oceanographic Institution, Woods Hole, MA 02543, U.S.A.
† Department of Applied Ocean Physics and Engineering, Woods Hole Oceanographic Institution, Woods Hole, MA 02543, U.S.A.

gained into the high-resolution distributional patterns of certain taxonomic groups (Holliday *et al.*, 1989). Such correlations between acoustical or non-imaging optical measurements and the actual taxonomic composition of the plankton are rough approximations at best, since there is much overlap between the various taxonomic groups in their acoustical and optical properties.

Recent advances in underwater optical imaging on small scales have allowed *in situ* observations of planktonic taxa to be made [e.g. Ecoscope, Kils (1992); J. R. Strickler's Critter-Cam, Bergeron *et al.* (1988); ROV deployed video, Paffenhofer *et al.* (1991); Video Profiler, Gorsky *et al.* (1992); the Video Plankton Recorder, Davis *et al.* (1992a, b); for reviews see Schultz *et al.* (1992) and GLOBEC (1993)]. Furthermore, rapid growth in the field of video image processing together with the dramatic increase in computing power has made possible analysis of video images and analysis/visualization of the resulting data in near-real time.

In the present paper, we describe a method for rapid visualization of the distribution of planktonic taxa while at sea. The method is based on our Video Plankton Recorder technology and involves a semi-automated technique of video analysis.

METHODS

System requirements

A fully automated at-sea analysis of plankton size and taxonomic composition requires three basic steps:

(1) High-quality images of individual plankton need to be obtained.

(2) An image processing and pattern recognition system must be developed for real-time processing of the large volume of image data being acquired. This processing includes three parts:

(a) a software/hardware system is needed for preprocessing of the images (including real-time image capture, object detection, focus detection, and digital storage of the region-of-interest [ROI]);

(b) pattern recognition algorithms must be developed for automated identification and classification of planktonic taxa;

(c) the pattern recognition algorithms must be transferred to high-performance image analysis hardware in order to achieve real-time processing capability.

(3) A data processing and visualization system must be developed to analyze and display the distributional data at sea in real-time.

We have accomplished the first step with the development of the VPR, which provides high-quality images that are well suited for subsequent image processing steps. We also have completed the development of the preprocessing system described in Step 2a and have used it to obtain ROIs of planktonic taxa in real-time while at sea. We are currently developing the automated pattern recognition algorithms described in Step 2b. When these are completed, we will upgrade our image processing hardware as needed (Step 2c). As an interim solution, we have developed a "point-and-click" user interface for analyzing ROIs obtained at sea and from archived video tapes. Although this system can be tedious to use (because of the large number of ROIs to analyze), it allows near real-time sorting of ROIs generated by our preprocessing system. We also have developed data processing software

that interfaces with commercial visualization software (Advanced Visual Systems, Inc.; AVS) (Step 3). In the following sections, we describe our methods for image acquisition, image analysis, and data processing/visualization.

Acquisition of video images

The Video Plankton Recorder (VPR) is an underwater video system with magnifying optics that can image particles in the size range of 10 microns to several centimeters (Davis *et al.*, 1992a, b). Two to four video cameras are configured to simultaneously view concentric volumes in either stereo or monoscopic mode at two or more magnifications. The cameras are synchronized at 60 fields per second (fps) to a red-filtered 80 W xenon strobe ($\simeq 1$ μs exposure). The VPR also includes a suite of auxiliary sensors including a CTD, fluorometer, transmissometer, and flowmeter. The system has been deployed in various configurations including towing, ROV studies, and fixed platform sampling. A moored, vertically profiling system is under development.

Data presented in this paper are from the towed VPR system, which consists of up to four video cameras with magnifying optics that can be adjusted to provide fields of view between 5 mm and 10 cm. Use of higher magnification lenses is currently being explored for viewing protozoans (~ 2 micron resolution). The four cameras are set for concentric viewing fields so a range of up to four magnifications can be viewed simultaneously, allowing a wide size range of plankton to be sampled. Depth of field is adjusted by the lens aperture setting, and the volume sampled in each video field ranges from 0.5 ml to 1 liter depending on lens settings.

The beam of red light from the strobe is expanded to 10 cm, collimated, and aimed obliquely past the cameras to provide dark-field illumination. Strobe-to-camera distance is 1.0 m with the viewing area at 0.5 m. Video data are telemetered to the surface via fiber optic cable and stored, together with time code overlay, using broadcast quality videotape recorders. Abundance is calculated from the video by counting the number of plankton per field and dividing by the field volume. The VPR was designed to minimize disturbance of the sampled volume in order to reduce possible disruption of the imaged particles or detection and avoidance by the plankton. Data from the auxiliary underwater sensors (CTD, fluorometer, transmissometer, and flowmeter) are acquired using the same underwater and deck electronics units as used on the MOCNESS (Wiebe *et al.*, 1987).

Analysis of video images

Live or recorded video together with time-code overlay is sent to the VPR's video processing system which consists of a SUN SPARCstation 20 model 72 connected to an Imaging Technologies Inc. model 151 pipeline image processor and a time-code reader (Horita, Inc.). The image processor can perform real-time (60 fps) field grabbing, convolutions, edge detection, and output of pixel coordinates to the host workstation. An algorithm has been developed to read the video time-code (field accurate) in real time from the time-code reader into the SUN. We have prototyped several techniques using the IT-151 pipeline processor for real-time presence–absence detection of plankton and for sending selected streaks from the region-of-interest (ROI) to the SUN for focus detection. The in-focus ROIs are sent from the IT-151 to the SUN hard-disk and compressed to Exabyte tape for storage.

The goal of the focus detection system is to archive to disk any images of sufficiently large, bright, and in-focus objects as they appear in the video stream. The pipelined image processing hardware digitizes, filters, and segments the imagery at 60 Hz. The image processor is controlled by a multiprocessor workstation, which logs time-coded images as well as hydrographic and navigation data.

A simple but effective algorithm is performed in real-time. First, bright targets are located. Then the edge strength (gray-scale gradient across the edge) along their perimeter is inspected to determine if they are in focus. A region of interest surrounding the in-focus target is immediately passed to the workstation where it can be taxonomically classified. This culling process typically reduces by a factor of 30 or more the amount of image data that needs to be stored and classified.

On average, about 1 out of 20–60 video fields contains an in-focus object that is saved to disk as an ROI file, a sub-image of the original field. Thus, about 1–3 ROI files are generated per second or about 3600–10,800 per hour, for a total of 21,600–64,800 ROIs for a typical 6-h tow. These ROI files are named using the corresponding video time code and are stored in a directory that is named according to VPR tow and camera number. At present, the focus detection system is not perfect. In areas of high particulate abundance, the system will skip some in-focus objects while processing others, thus underestimating abundance. We are currently in the process of quantifying this error for data already collected and are upgrading the hardware so that all in-focus particles will be detected.

The ROIs are sorted according to taxonomic category, and the individual object widths are measured using a "point-and-click" user interface written in Matlab (Mathworks, Inc.). The list of ROI files contained in each subdirectory is used to input each ROI as an image file into a Matlab figure window. The window also contains a list of categories from which the type of the current object can be selected. Once the category is selected, the user can measure the width of the object, enter a comment, or go to the next ROI. The time code, category name, object width, and comment are written to an output file.

Data processing and visualization

To determine the spatial distribution of each taxon, the individual entries in the output file are sorted by taxa using a Matlab routine, and the time code corresponding to each individual organism is binned into 2-s intervals time-matched to the VPR hydrographic collection interval. (The example data given below are binned into 4-s intervals since they were collected with an earlier VPR system in which the hydrographic collection interval was 4 s). The VPR time-code and hydrographic times are synchronized using Geosynchronous Positioning Satellite (GPS) data. Latitude and longitude from the GPS together with GMT are written together with the ancillary data (including VPR depth) every 2 s. In this way, the VPR depth, latitude, longitude, and number of individuals per taxon observed during each 2-s interval along the VPR tow path are recorded. The volume imaged per 2-s interval is constant since the tow speed is high enough that adjacent video fields do not overlap. The volume per field is determined from the field height, width, and depth of field [see Davis *et al.* (1992a) for details of calibration method].

After the data for each taxon are in the form of latitude, longitude, depth, and abundance (no. l^{-1}) for each 2-s interval, the data are ready for input into the visualization programs. Straight transect data are gridded in two dimensions (i.e. depth and distance) and input to Matlab for contouring vertical sections. The NCAR Zgrid operator, $\nabla^2 - 3\nabla^4$, was used for

gridding. Distributions in 3-space are input directly into AVS for rendering. In the latter case, the four-column data (x, y, z, abundance) are viewed in two ways. The data can be viewed directly, without interpolation, as "bubbles" in 3-space (AVS routine Bubblevis) where abundance in each 2-s interval is proportional to bubble size and color. The data also can be linearly interpolated as uniform cell data (UCD) and displayed using UCD volume rendering and animation routines.

CD-ROM—an example of the image analysis steps including real-time ROI extraction and rotating rendered volumes of *Calanus finmarchicus* and fluorescence distributions from the grid are displayed on the CD-ROM accompanying this volume. The reader is strongly encouraged to view the video sequence, since it demonstrates the speed of the real time analysis and aids in the interpretation of the static 3-D figures.

Field sampling

As an example of the kind of information obtainable from the VPR system, data are presented from a tow made during GLOBEC cruise R.V. *Columbus Iselin* (CI9407) to Georges Bank on 25 May–16 June 1994. During this cruise, VPR towyos were made either along a straight transect or along a square inward spiral (i.e. a grid) centered on a drifter (drogue at 10 m). Data presented in this paper are from a ~6-h towyo (VPR 9) made using the spiral tow pattern, which, after subtracting out the movement of the drifter, yielded a 2×2 km $\times$ 90 m grid (Fig. 1). The complete towyo path consisted of 47 double oblique profiles. To follow this grid with the ship, a sheet of acetate with the square spiral on it was placed on the ship's radar scope, and the ship steamed so that the drifter's reflection on the radar scope moved along the spiral path of the grid from the outermost corner towards the center. (A counter-clockwise spiral was used because the VPR was towed off the port side using the crane boom, and sharp starboard turns could not be made because the wire would have run under the stern of the ship and come too close to the propeller.) The position of the drifter was determined from a GPS receiver and ARGOS transmitter on the drifter. Sampling of the grid started at 2308 (Eastern Daylight Time) on 30 May at 41°35.374′N and 66°6.955′W and ended at 04:33 on 31 May at 41°35.410′N and 66°11.448′W (5.42 h total time). The drifter moved westward for 6.1 km.

Video images from two cameras were analyzed. Camera 4, the high-magnification camera, was set for a field of view of 6.0×4.5 mm and a depth of field of 23 mm. Camera 2, a low magnification camera, had a field of view of 34×24 mm and a depth of field of 40 mm. Thus, the imaged volumes in this study for cameras 4 and 2 were 0.6 and 33 ml, respectively. Since each video field contains a new volume, new volumes are sampled at 60 Hz, so the total volumes sampled per hour are 130 and 7128 l for cameras 4 and 2, respectively.

Although these sampled volumes appear small relative to the volume sampled by a plankton net, the number of abundant organisms actually counted in plankton net samples (typically ~1000 total individuals) is similar to or less than the number counted by the VPR for tows of comparable duration. This similarity is due to the fact that abundant taxa in plankton net samples are subsampled down to a manageable (=countable) number of organisms. Thus, the volume imaged by the VPR along its tow path, can be thought of as a subsample of the volume that would be sampled by a plankton net traveling along the same tow path. In this way, the VPR collects images of the plankton that would have occurred in a plankton net subsample, without having to make the net collection or do the subsampling. Furthermore, the VPR provides information on the spatial distribution of the plankton

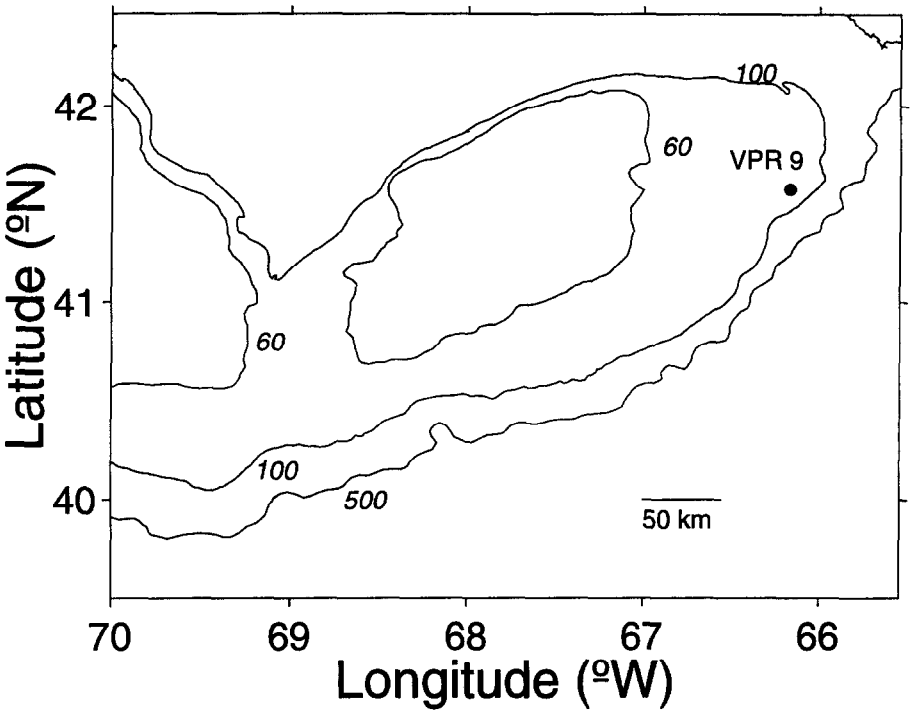
100
60
VPR 9
60
100
500
50 km
42
41
40
Latitude (ºN)
70
69
68
67
66
Longitude (ºW)

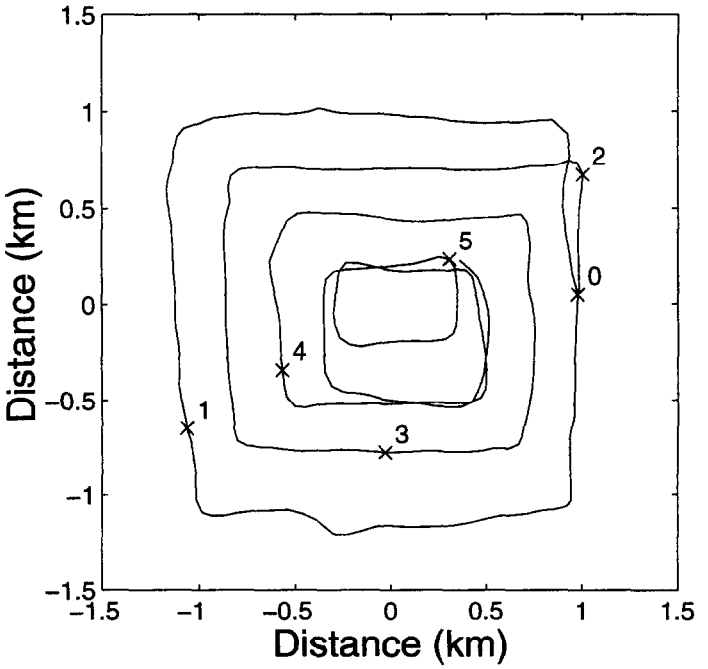
1.5
1
0.5
0
−0.5
−1
−1.5
Distance (km)
2
5
0
4
1
3
−1.5
−1
−0.5
0
0.5
1
1.5
Distance (km)

along the tow path. In this analogy, the VPR will provide an unbiased estimate of the mean abundance (like taking a random core through the cylinder of the net path) even when the organisms have a patchy distribution, although in the latter case the variability of repeated subsamples would be greater (A. R. Solow, WHOI, personal communication, 1995). For this reason, the agreement in abundance estimates between MOCNESS and the VPR are very close for abundant taxa (Benfield *et al.*, 1996). On the negative side, the total volume imaged by the VPR is much smaller than that of a plankton net, so that rare organisms ($< 10\ m^{-3}$), which are present in a net sample, are undersampled by the VPR (see also, Benfield *et al.*, 1996). This undersampling is due to the limitations of resolution on current CCD chips. To identify and count the same number of organisms collected by a $1\ m^2$ plankton net would require a CCD chip with 100 x 100K pixels (i.e. a field of view of $1\ m^2$ with the same resolution as camera 4). Such chips are not currently available (but should be within the next few years), but we are presently incorporating higher resolution CCD arrays into the VPR to increase our sampling volume.

RESULTS AND DISCUSSION

Using the VPR/image-processing system, one of us (CD) was able to analyze all the ROIs from Cameras 2 and 4 within 12 h after the grid was sampled and visualize the distributional data. Thus, this technique saves literally hundreds of hours in sample processing time over conventional methods and allows near real-time visualization of the plankton distributions while at sea. At present, the only other way to sample distributions of plankton taxa in a volume of ocean this size with high resolution, would be to use an LHPR (cf. Wiebe, 1970). An LHPR towyoed along the same path as the VPR, however, would integrate over scales of 5–10 m and would generate hundreds of samples requiring many weeks or months to analyze. The new technology described here allows one to quickly and routinely view volumes of ocean and gain immediate insight into the spatial distributions of plankton and other particulate matter contained therein. The combination of such observations with data from ancillary environmental sensors on the VPR allows rapid insights into the spatial relationships of plankton with important elements of their environment. As an example, of such insights, we present data from the 2-km grid sampled in May 1994.

Temperature, salinity, density, fluorescence, and beam attenuation all exhibited a gradient from east to west across the grid, so that, as the spiral towyo progressed, damped oscillations in the vertical distributions of these variables were observed during the first 5 h (Fig. 2). Given the relatively close proximity of the shelf/Slope Water front (typically coinciding with the 100 m isobath; Fig. 1), the deeper, saltier water may have originated from cross-frontal mixing with the adjacent Slope Water. Although both the horizontal and vertical gradients were distinct, they were weak. The water column was only weakly stratified in temperature (7.8–6.6°C) and salinity (32.9–33.3 psu) from bottom to surface. Interestingly, near the end of the towyo, a large downward displacement of the pycnocline was observed and was associated with a deepened thermocline and fluorescence maximum.

Fig. 1. Upper panel: map of study area showing the starting position of VPR tow 9 on the northeast peak of Georges Bank (bathymetry in meters). During the tow, the drifter moved westward for 6.1 km. Lower panel: plan view of VPR track along the square inward spiral grid. The track is relative to the drifter position and is marked at hourly intervals (x-axis is east–west, y-axis is north–south).

Table 1. *Categories of planktonic taxa observed in high-magnification camera (Camera* 4*). Total number of organisms counted and mean abundance over the entire grid are also shown. (Total volume sampled over the grid* = 7421 *for Camera* 4*)*

Taxon	Number counted	Mean Abundance (no. m^{-3})
Marine Snow	897	1209
Diatom, *Chaetoceros* sp.	709	955
Diatom, *Chaetoceros socialis* colonies	666	897
Diatom, *Coscinodiscus* sp.	272	366
Unidentified Copepods	179	241
**Calanus finmarchicus*	150	202
Diatom, rod-shaped (no observable spines)	150	202
Unidentified objects	88	118
Pseudocalanus spp.	35	47.2
Pseudocalanus with eggs	26	35.0
Larvaceans	10	13.5
Copepod Nauplii	6	8.1
Oithona	6	8.1
Dinoflagellate, *Ceratium*	6	8.1
Echinoderm Larvae, Ophiopluteus	5	6.7
Medusae, unidentified	4	5.4
Medusae, hydroid	3	4.0
Oithona with eggs	2	2.7
Ctenophores	2	2.7
Polychaete larvae	1	1.4
Pteropods	1	1.4
Total	3218	4337

*Note *Calanus finmarchicus* abundances shown in this table are from Camera 4; Camera 2, because of its larger sample volume, was used to determine *C. finmarchicus* abundance shown in Fig. 4.

This feature was well sampled by the large number of vertical profiles (10 individual profiles) that passed through it. Because this physical and biological feature occurred near the end of the towyo, its position in space was at the center of the grid.

Using AVS visualization software, we see clearly the tilting thermocline across the grid and the deepened warm-temperature plume at the center of the grid (Fig. 3a). The salinity gradient across the grid was steeper than that for temperature (Fig. 3b). The isohaline surface reveals that the cross-grid gradient occurred well down into the water column on the eastern side. A fluorescence gradient also occurred across the grid (Fig. 3c) with higher fluorescence on the eastern side where the thermo- and haloclines were deeper. As is suggested by the time plot (Fig. 2), high fluorescence is associated with the warm plume in the center of the grid. This plume is difficult to see in Fig. 3c, but can be seen clearly in the video animation of fluorescence on the accompanying CD-ROM.

The plankton observed in the high-magnification camera (Camera 4) spanned 21 categories comprising phytoplankton, zooplankton, and detritus (Table 1). Camera 2 video was analyzed for *Calanus finmarchicus* abundance only. A total of 1952 individual *C. finmarchicus* were counted from Camera 2. As shown in Table 1, the dominant categories observed in Camera 4 are marine snow, diatoms, unidentified copepods, and *C. finmarchicus*. Many of the unidentified copepods may be younger life stages of *C. finmarchicus* that were difficult to distinguish because of body orientation.

Calanus finmarchicus abundance (determined from camera 2) was highest on the western half of the grid near the surface (Fig. 4a). This general pattern also can be seen using the AVS Bubblevis module where bubble size and color are proportional to *C. finmarchicus* abundance (Fig. 4b). Although the distributional patterns are quite similar in Fig. 4a and b, the linear tetrahedral interpolation used in Fig. 4a fills in the spaces between the data points to generate the UCD structure, resulting in smoothed distributions. The pattern of *C. finmarchicus* abundance is in direct contrast to the distribution of fluorescence and many of the diatom groups that had higher concentrations on the eastern half of the grid. It is possible, given the concentrations of *C. finmarchicus* ($\sim$200–900 ind./m^3), that grazing ($100\,ml^{-1}\,ind.^{-1}\,h^{-1}$, Mullin, 1963) could have been responsible for the reduced fluorescence and diatom numbers, but the corresponding gradients in temperature and salinity suggest that a physical process may have contributed to the observed biological gradients. *C. finmarchicus* was observed in highest concentrations near the ocean surface. Another way to visualize the spatial relationships between fluorescence and *C. finmarchicus* is to merge the two distributions together into the same volume and again use the AVS Bubblevis module to display *C. finmarchicus* abundance where bubble size is proportional to abundance (Fig. 4c). A *t*-test confirmed that the ratio of *C. finmarchicus* abundance to fluorescence was nearly twice as high on the western half of the grid than on the eastern half ($P < 0.99$).

Given that it is inherently difficult to see these distributions in 3-space solely from the figures presented in this paper, we also have included on the accompanying CD-ROM short animations of Fig. 3c and 4a. In these animations, the volumes are rotated from a top view to a side view, followed by a 360° horizontal rotation and a vertical rotation to the original top-view position.

Several of the groups were extremely fragile and would have been difficult or impossible to sample using traditional instrumentation. This was particularly true for two of the most abundant groups, *Chaetoceros socialis* colonies (Fig. 5a) and marine snow. The *C. socialis* colonies (1–4 mm colony length) were so abundant during two other VPR tows on the cruise that the video monitor for the high magnification camera became saturated with images of these organisms, and the fluorometer readout also became saturated. Saturation of the video screen lasted a few seconds, during which no quantitative counts of plankton could be made in this camera. Lower magnification cameras did not become saturated, so that colony abundance still could be quantified using these cameras. These colonies are important components of the Georges Bank system, but until now there has been no adequate method to determine their abundance and distributions. Images of these colonies are presented in Gallager *et al.* (1996). We found that they are fragmented when sampled through the spigot at the bottom of a Nisken bottle and totally destroyed by net and pump sampling. They are likely responsible for net clogging throughout much of Georges Bank, since we observed a green mucilaginous coating on the clogged MOCNESS nets in regions where *C. socialis* colonies were abundant.

Other diatoms also were abundant, including a straight-chain species of *Chaetoceros* (1–3 mm chain length) having long spines (Fig. 5b), the centric diatom *Coscinodiscus* sp. (0.5 mm diameter) (Fig. 6a), and a rod-shaped chain-forming diatom with no observable spines (1–4 mm chain length) (Fig. 6b). The straight-chain *Chaetoceros* species had a distributional pattern similar to the *C. socialis* colonies, with highest concentrations on the eastern half of the grid where the fluorescence was higher (Fig. 5b). Given the high concentrations of both these groups, it is likely that they contributed a substantial portion of

the total fluorescence signal. However, their actual contributions require further analysis of fluorescence per cell for these groups relative to other phytoplankton species collected by bottles, but too small to be seen with the VPR. All diatom species were much more abundant in the upper half of the water column especially near the surface (Figs 5 and 6). During a VPR tow in the northern part of the well-mixed area, the video monitor again became saturated, this time because of the rod-shaped diatoms. Species identification of these groups will be obtained from future analysis of the Nisken samples collected in these regions.

Marine snow was the most abundant group observed (Fig. 7). As viewed with the video, the marine snow imparted a 3-dimensional particulate structure to the water, which was rather terrestrial in appearance at these small scales (like trees in a forest). Certainly the ocean appears far different when viewed directly at these scales than it does by inferences drawn from traditional net and bottle collections in which the natural particulate structure is destroyed by sampling. Marine snow was most abundant in the lower half of the water column. It is possible that these particles result from decomposition of sinking *C. socialis* colonies (see Norrbin *et al.*, 1996). Visual observation of the video from many subsequent VPR tows reveals that the concentrations of marine snow on Georges Bank varies greatly in time and space and that the abundance of snow in this tow appears much lower than in many other tows. Nonetheless, marine snow was nearly always the most abundant particulate matter observed. Future data analysis will address the temporal and spatial patterns of marine snow abundance. Because marine snow scatters light well, the focus detection algorithm works well for these particles.

Both physical and biological structure of the volume of seawater exhibited gradients across the grid. As mentioned above, the sampled region of Georges Bank is near the shelf/slope edge of the bank, and mixing of water masses is a possible explanation for the observed salinity gradients. Weak vernal thermal stratification also was apparent. Grazing by *C. finmarchicus* could account for the lower phytoplankton levels on the eastern portion of the grid. The cause of higher *C. finmarchicus* abundance on the western portion of the grid is uncertain and must await a more complete analysis of the data from the cruise, including ADCP current measurements and hydrography.

The data from this VPR towyo were presented as an example to show the kind of rapid insights about a region of the ocean that can be obtained using a high-resolution optical imaging system together with image processing techniques developed thus far. Although the particular volume sampled had fairly weak gradients (as was expected in that location at that time of year), other regions, such as the shelf/slope front, or other times of year, such as summer, have much stronger gradients. The seasonal evolution of stratification and frontal development on Georges Bank is being intensively studied in the current GLOBEC field program. The VPR system is providing insights into the planktonic environment while at sea. Such rapid assessments are helping to direct rate-process sampling as well as provide time series of 2- and 3-dimensional snapshots of the dynamical pelagic environment.

In conclusion, the emerging field of underwater optical imaging [for reviews see Schultz *et al.* (1992) and GLOBEC (1993)], when combined with the rapidly growing fields of image processing and data visualization has the potential to provide major new scientific insights in Biological Oceanography. These powerful new tools will allow oceanographers to view the planktonic environment quickly and non-invasively over a broad range of scales (from the individual to the population).

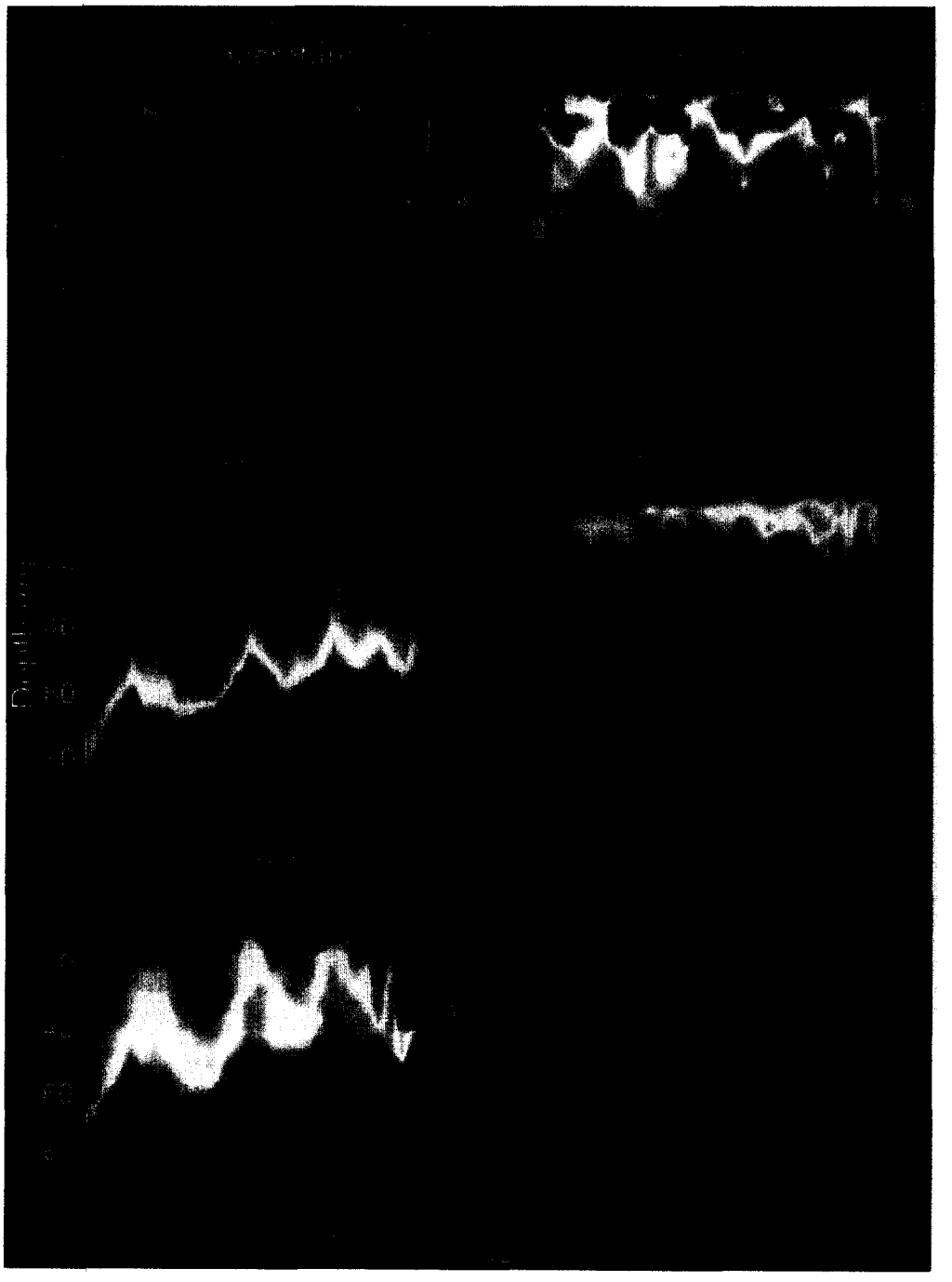

Fig. 2. Vertical sections of data from the CTD, fluorometer, and transmissometer along the VPR towyo path shown in the lower right panel. The x-axis is plotted as time since the start of the tow. The track of the towyo in x–y space is shown in Fig. 1. Note the damping of the oscillations in the vertical structure of the variables (e.g. salinity) followed by the deepened surface plume near the end of the towyo.

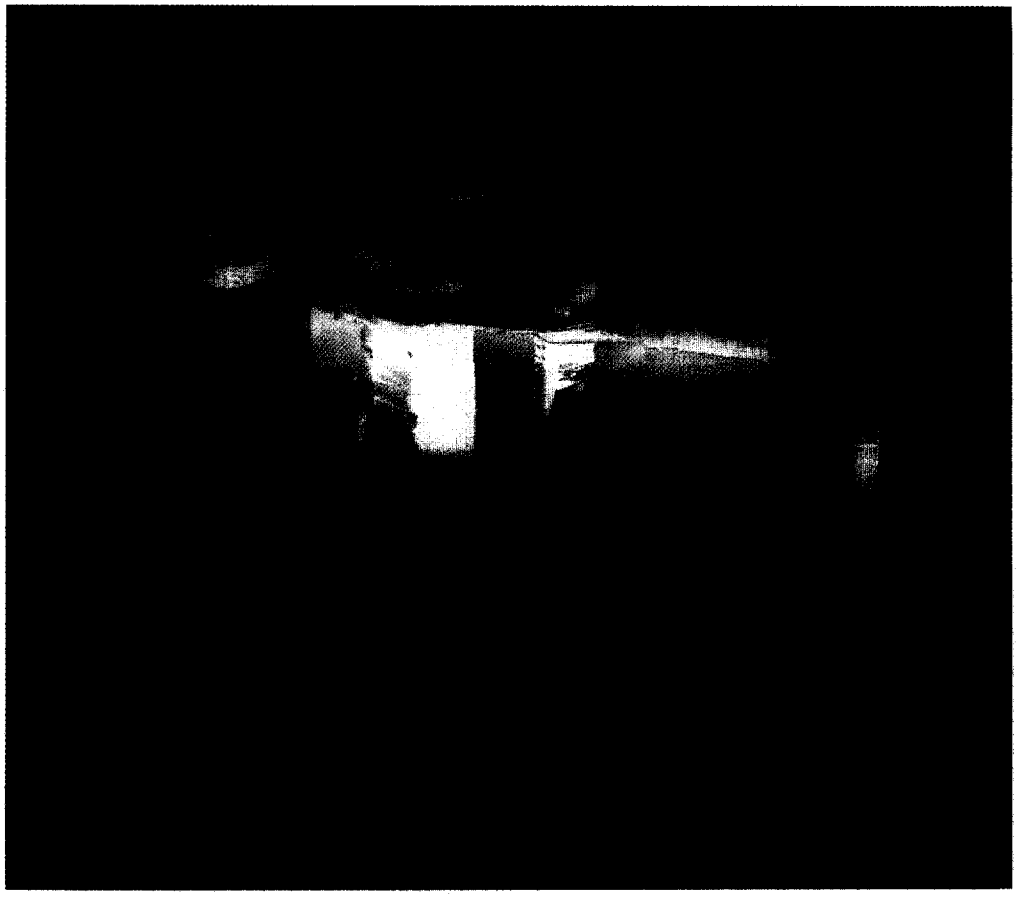

Fig. 3. (a) Volume rendered temperature data from the towyo/grid using the AVS visualization software to display the data as uniform cell data (UCD). As indicated in Figs 1 and 2, the volume dimensions are 2×2 km $\times 90$ m deep. West is toward the left and south is toward the reader. The isosurface was chosen to correspond to the thermocline temperature. The color of the volume represents temperature and is rendered translucent for viewing the isosurface. Note the cross-grid slope of the isothermal surface and the warm plume at the center of the grid as was suggested in the time plot (Fig. 2). (Note that for clarity only one isosurface is shown for each plot, but that interactive visualization allows dynamic adjustment of the isosurface levels. In general, the higher valued isosurfaces are circumscribed by the lower valued ones, so that, for example the higher fluorescence surfaces would stack on top of the one shown here and would diminish in areal extent. The triangular shapes of the surfaces are due to the nature of the UCD tetrahedral structure in which irregularly spaced data in the volume form the nodes of the tetrahedra.)

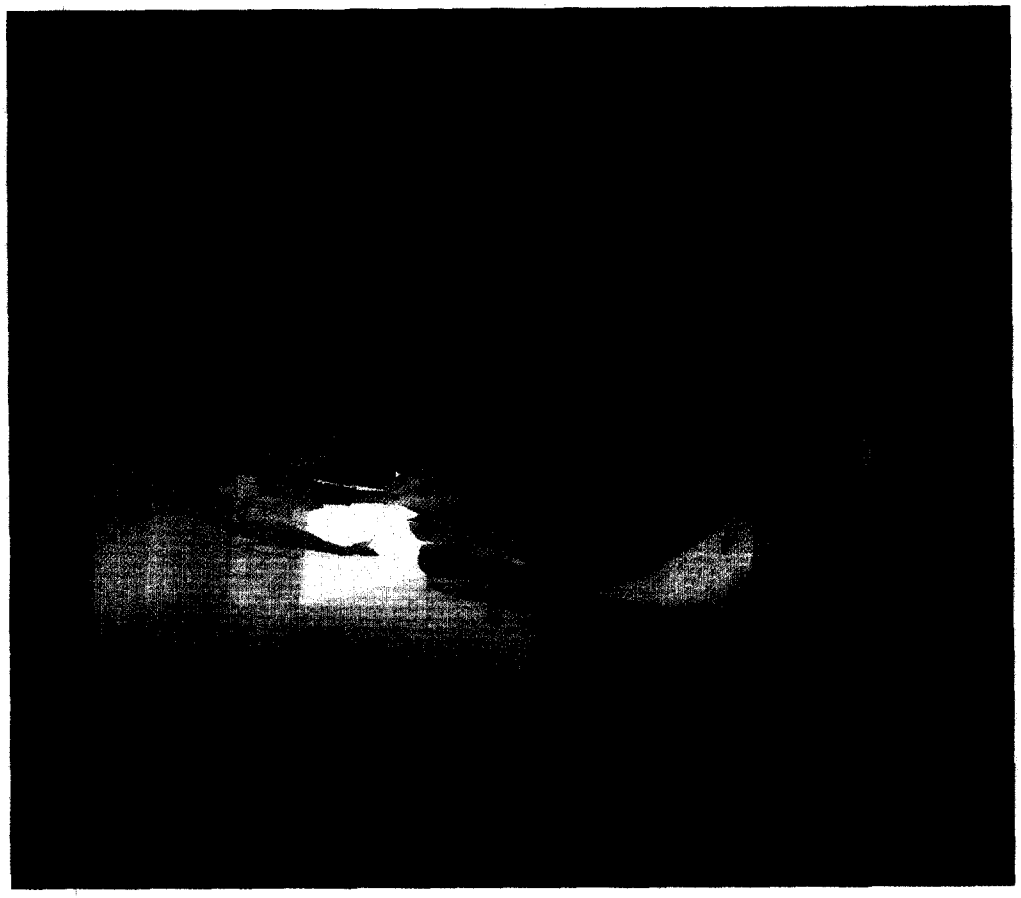

Fig. 3. (b) As (a) but for salinity. Note the large slope of the isosurface. [Note also that the volume is rotated clockwise about 45° from that shown in (a).]

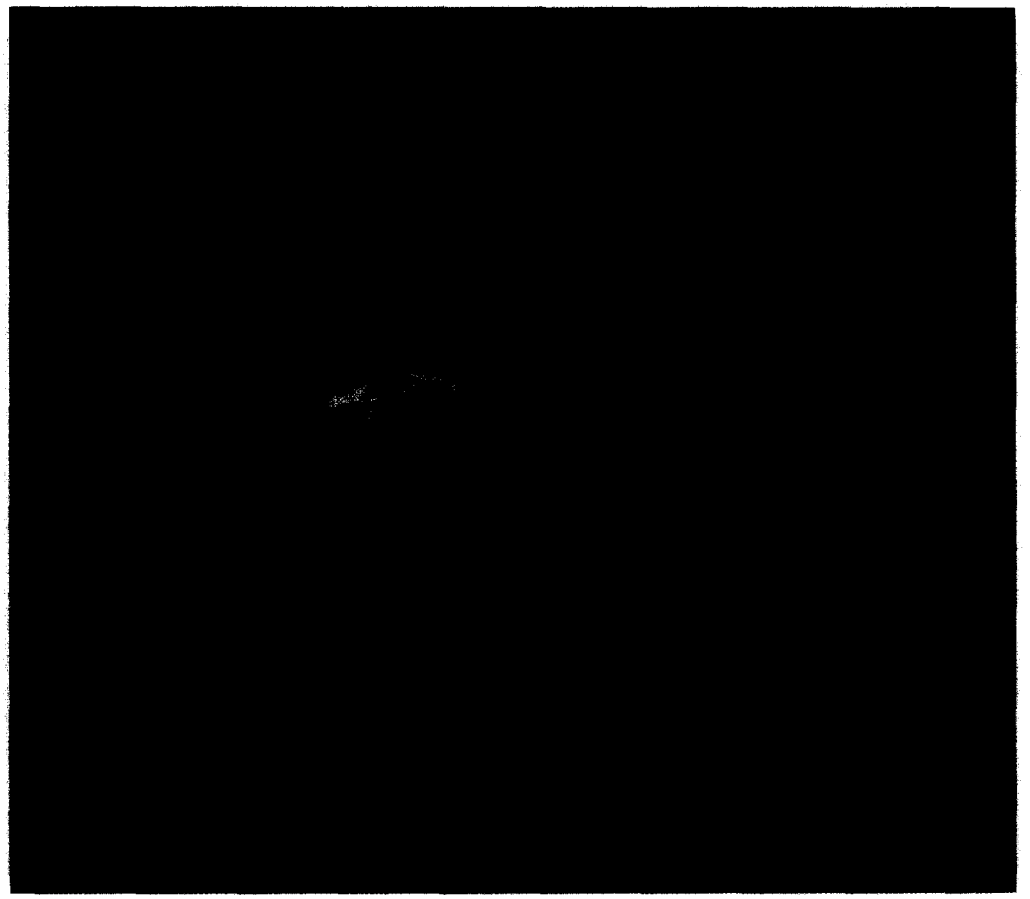

Fig. 3. (c) As (a) but for fluorescence. Note the higher concentration of fluorescence on the eastern half of the grid near the surface. [Note also that the volume is rotated clockwise about 45° from that shown in (a).]

Fig. 4. (a) The distribution of *Calanus finmarchicus* over the grid showing higher concentrations on the western half of the grid. Plot rendered as in Fig. 3. Volume dimensions and view angle as in Fig. 3a.

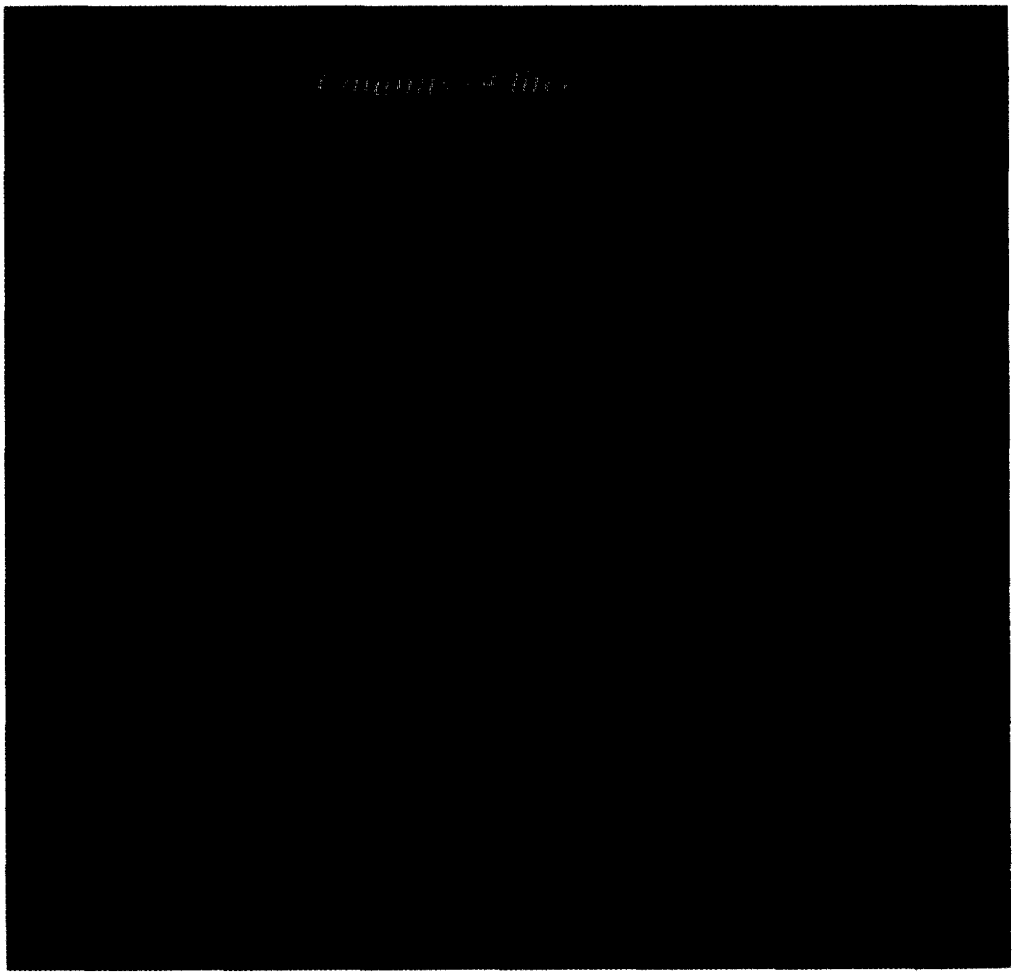

Fig. 4. (b) For comparison with panel (a), the abundance of *Calanus finmarchicus* in each 4-s interval is represented by bubble size and color using the AVS module Bubblevis. Depth cuing also was used in the visualization so that bubbles further away from the viewer are paler, simulating fogginess. Note the similarity in the distribution of the isosurface in (a) with the higher concentrations of *Calanus* shown in (b). Note also that the UCD trianglar interpolation causes the isosurface to fill in spaces between the bubbles giving a smoothed distribution.

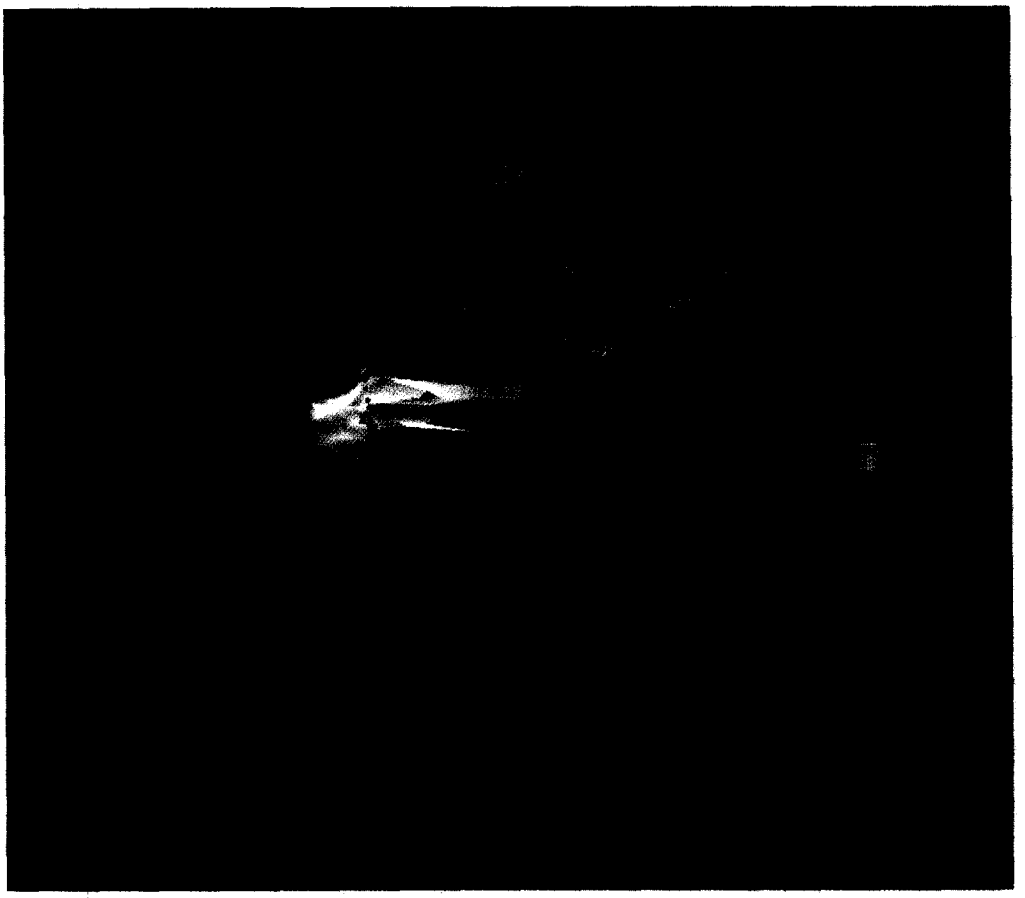

Fig. 4. (c) The distributions of fluorescence and *C. finmarchicus* superimposed in a single volume using the AVS module Bubblevis to display the *C. finmarchicus* abundance as proportional to bubble diameter. The volume and isosurface are for fluorescence as shown in Fig. 3c.

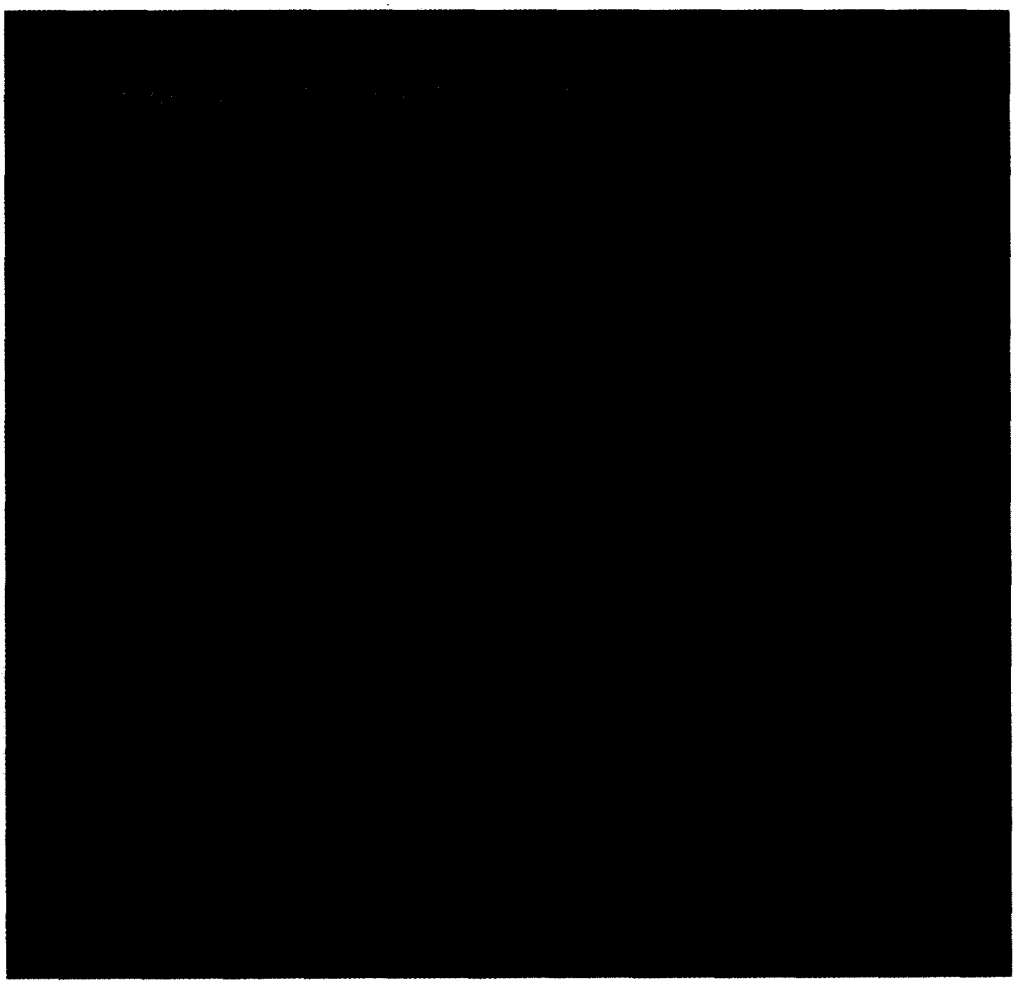

Fig. 5. (a) Distribution of diatoms, *Chaetoceros socialis* colonies. Note higher concentrations near the surface on the eastern half of the volume as was the case for fluorescence (Fig. 3c). (Plotting method as in Fig. 4b.)

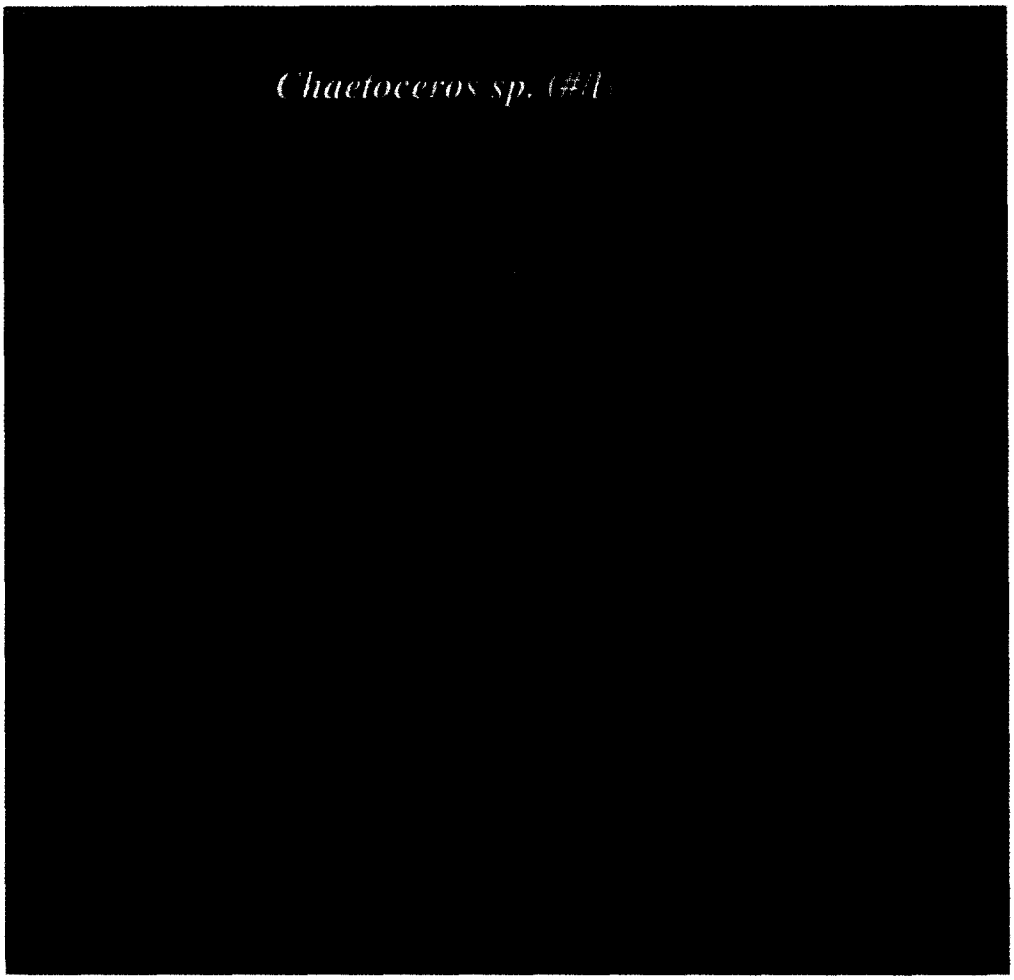

Fig. 5. (b) Distribution of diatoms, a straight chain *Chaetoceros* with long spines. Note higher concentrations near the surface on the eastern half of the volume as was the case for fluorescence (Fig. 3c). (Plotting method as in Fig. 4b.)

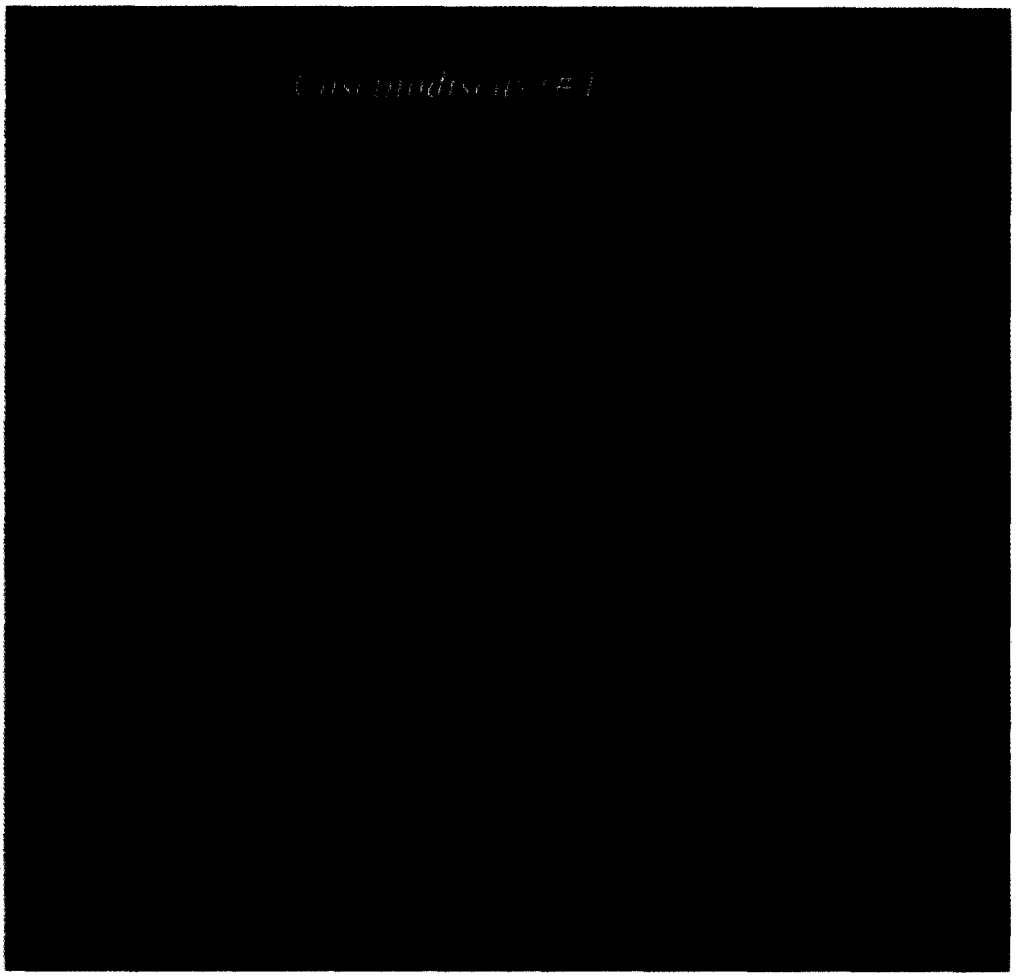

Fig. 6. (a) Distribution of the diatoms *Coscinodiscus* sp. Note higher concentrations in the upper half of the volume. (Plotting method as in Fig. 4b. Note also the effect of depth cuing is more noticable in these figures than in Fig. 4b.)

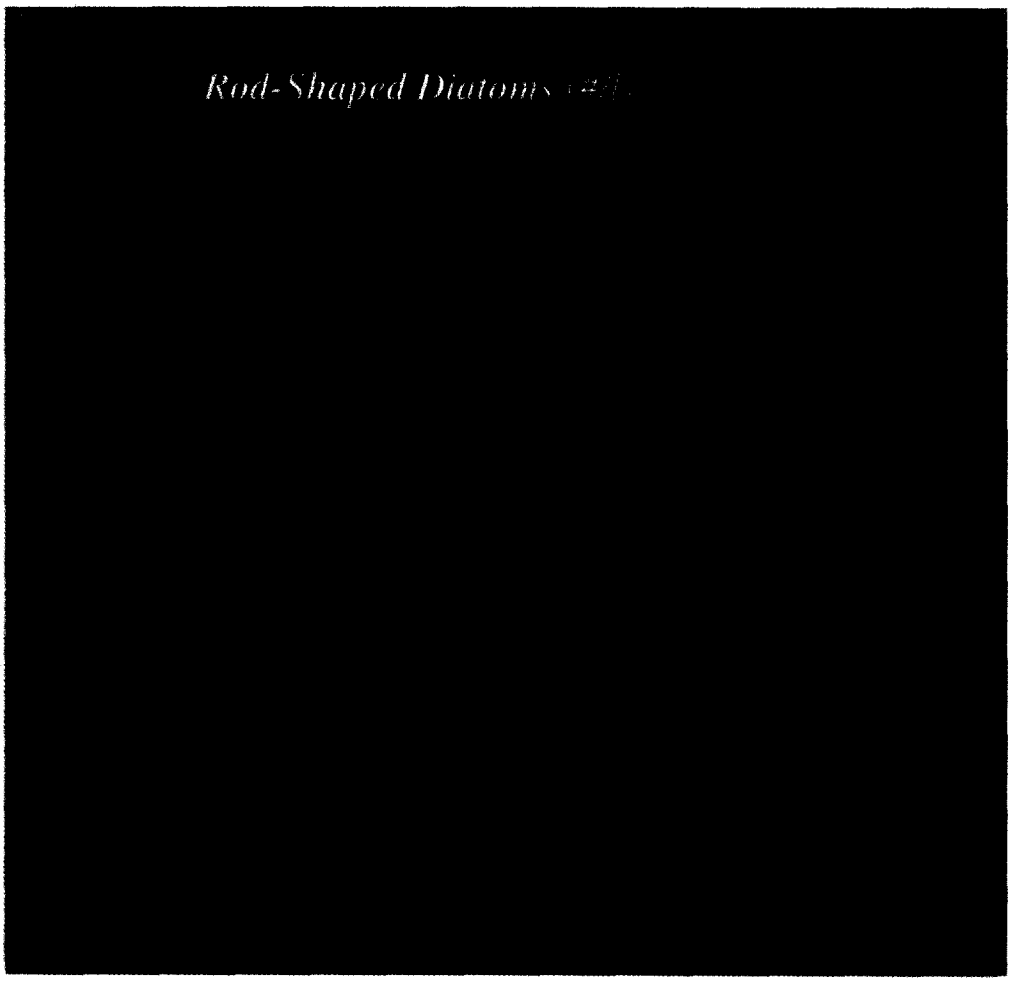

Fig. 6. (b) Distribution of a rod-shaped diatom without noticeable spines. Note higher concentrations in the upper half of the volume. (Plotting method as in Fig. 4b. Note also the effect of depth cuing is more noticeable in these figures than in Fig. 4b.)

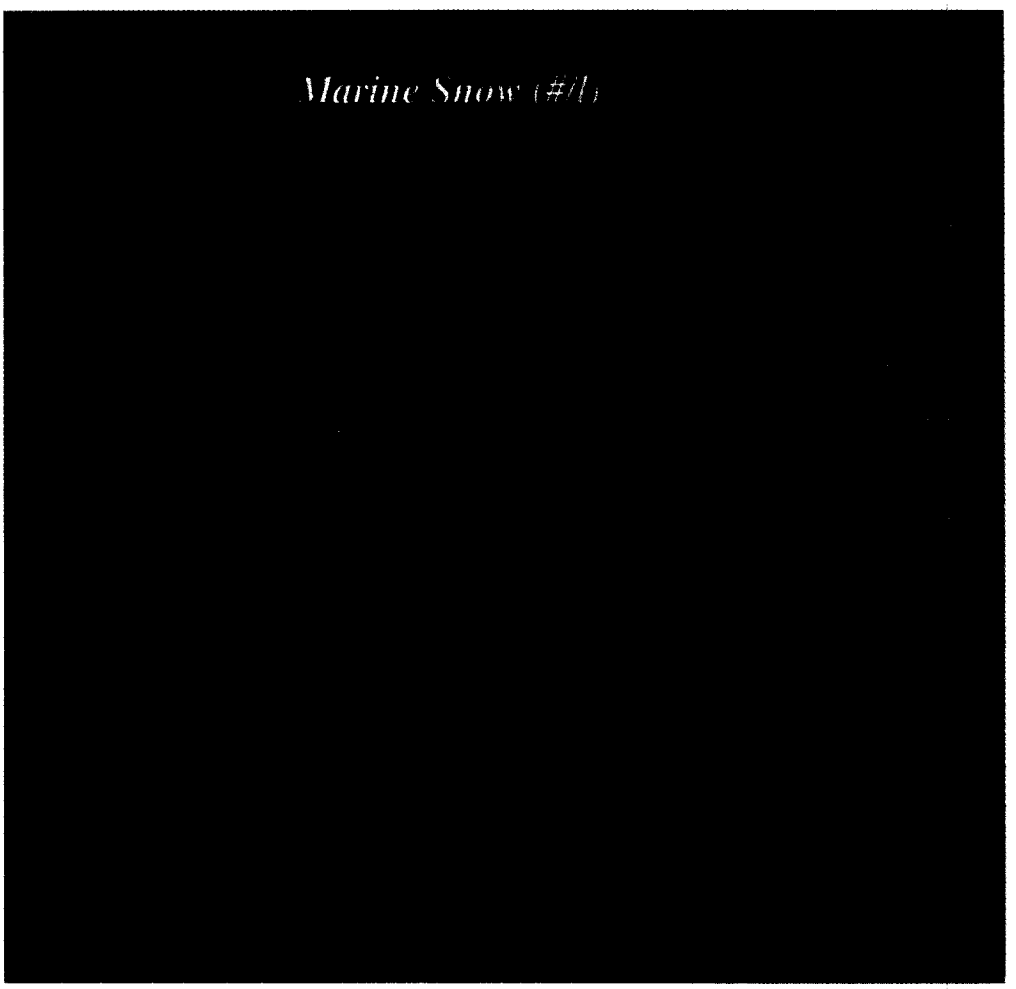

Fig. 7. Distribution of marine snow. Note higher concentrations in the bottom half of the volume. (Plotting method as in Fig. 4b.)

CD-ROM DESCRIPTION: IMAGE PROCESSING AND VISUALIZATION

Video fields are digitized in real time (60 fps), but only about 1 out of 20 contain an object of interest; the rest contain small or out-of-focus objects. To expedite processing of the digitized images, a method of automatic focus detection was developed. This was followed by manual sorting of images and visualization of the resulting distributions. This process is depicted in the following video sequences.

(1) A grey-scale image of a planktonic organism (Pteropod in this case) as digitized by the IT 151 image processor.

(2) The image is thresholded, all pixels above a certain grey level are shown in red and white.

(3) The edge is detected and focus level is determined along perimeter of organism and the region of interest (ROI) containing the organism is saved to disk.

(4) The focus detection can be done in real time. A workstation screen is shown with real-time video input in lower right and in-focus regions of interest being sorted and displayed in upper left. ROI extraction from the high magnification camera is shown first followed by the lower magnification camera. Note in the low magnification ROI extraction, the large number of *Calanus* observed during passage of the VPR through a patch of this copepod.

(5) Once the ROIs have been saved to disk, a Matlab point-and-click routine is used to manually sort the organisms to taxonomic group and measure their size. Sorting of ROIs from high magnification camera is shown first, followed by sorting of *Calanus* at low magnification. In the latter case, size was not measured, and the sorting was rapid and could keep up with real time.

(6) This semi automated method was used to analyze VPR images from a 2×2 km grid on Georges Bank in May 1994. The grid was centered on a drifter and the VPR was towyoed along the path in a square inward spiral. Tow depth was ~ 90 m.

(7) Visualization of the distribution of Calanus in the 2×2 km $\times 90$ m volume. Isosurfaces of 250 animals m^{-3} are shown. *Calanus* was most abundant on western side of the grid.

(8) Visualization of fluorescence. Fluorescence was highest on eastern side of grid. Given the observed concentrations of *Calanus*, grazing by these animals could have been responsible for the lower concentrations of phytoplankton on the western half of the grid.

Acknowledgements—We appreciate the assistance of the captain and crew of the R.V. *Colombus Iselin*. R. Signell provided help with the animations. This research was funded by NSF GLOBEC grant OCE9313671 and ONR grant N00014-93-1-0602. This paper is contribution number 61 of the U.S. GLOBEC program and WHOI contribution number 9092.

REFERENCES

Benfield M. C., C. S. Davis, P. H. Wiebe, S. M. Gallager, R. G. Lough and N. J. Copley (1996) Video Plankton Recorder estimates of copepod, pteropod and larvacean distributions from a stratified region of Georges Bank with comparative measurements from a MOCNESS sampler. *Deep-Sea Research II*, **43**, 1925–1945.

Bergeron E., A. D. Bowe, W. J. Hersey, W. N. Lange and J. R. Strickler (1988) Reaching the ultimate goal: observing live zooplankton *in situ*. *EOS*, **69**, 1087.

Davis C. S., G. R. Flierl, P. J. Franks and P. H. Wiebe (1991) Micropatchiness, turbulence, and recruitment in plankton. *Journal of Marine Research*, **49**, 109–151.

Davis C. S., S. M. Gallager, M. S. Berman, L. R. Haury and J. R. Strickler (1992a) The Video Plankton Recorder (VPR): design and initial results. *Archiv fèur Hydrobiologie Beiheft, Ergebnisse der Limnologie*, **36**, 67–81.

Davis C. S., S. M. Gallager and A. R. Solow (1992b) Microaggregations of oceanic plankton observed by towed video microscopy. *Science*, **257**, 230–232.

Denman K. L. and A. E. Gargett (1995) Biological/physical interactions in the upper ocean: the role of vertical and small-scale transport processes. *Annual Reviews of Fluid Mechanics*, **27**, 225–255.

Denman K. L. and D. L. Mackas (1977) Collection and analysis of underway data and related physical measurements. In: *Spatial patterns in plankton communities*, J. H. Steele, editor, Plenum Press, NY, pp. 85–109.

Gallager S. M., C. S. Davis, A. W. Epstein, A. Solow and R. C. Beardsley (1996) High-resolution observations of plankton spatial distributions correlated with hydrography in the Great South Channel, Georges Bank. *Deep-Sea Research II*, **43**, 1627–1663.

GLOBEC (1993) Inter national GLOBEC: Sampling and Observational Systems. Workshop report, IOC, UNESCO, Paris, March, 1993.

Gorsky G., C. Aldorf, M. Kage, M. Picheral, Y. Garcia and J. Favole (1992) Vertical distribution of suspended aggregates determined by a new underwater video profiler. *Annales de l'Institut océanographique*, Paris, **68**, 275–280.

Herman A. W. (1988) Simultaneous measurement of zooplankton and light attenuance with a new optical plankton counter. *Continental Shelf Research*, **8**, 205–211.

Holliday D. V., R. E. Pieper and G. S. Kleppel (1989) Determination of zooplankton size and distribution with multifrequency acoustic technology. *Journal du Conseil Internationale d'Exploration de la Mer*, **41**, 226–238.

Kils U. (1992) The ecoScope and dynIMAGE: microscale tools for *in situ* studies of predator prey interactions. *Archiv fèur Hydrobiologie Beiheft, Ergebnisse der Limnologie*, **36**, 83–96.

Marine Zooplankton Colloquium (1989) Future marine zooplankton research—a perspective. *Marine Ecology Progress Series*, **55**, 192–206.

Mullin M. M. (1963) Some factors affecting the feeding of marine copepods of the genus *Calanus*. *Limnology and Oceanography*, **8**, 239–250.

Norrbin M. F., C. S. Davis and S. M. Gallager (1996) Differences in fine-scale structure and composition of zooplankton between mixed and stratified regions of Georges Bank. *Deep-Sea Research II*, **43**, 1905–1924.

Paffenhofer G. A., T. B. Stewart, M. J. Youngbluth and T. G. Bailey (1991) High-resolution vertical profiles of pelagic tunicates. *Journal of Plankton Research*, **13**, 971–981.

Platt T. and K. L. Denman (1978) The structure of pelagic marine ecosystems. *Rapports et Procès-Verbaux des Reunion Conseil Internationale d'Exploration de la Mer*, **173**, 60–65.

Schultz *et al.* (1992) *Archiv fèur Hydrobiologie Beiheft, Ergebnisse der Limnologie*, **36**, 1–21.

Sheldon R. W., A. Prakash and W. H. Sutcliff Jr (1972) The size distribution of particles in the ocean. *Limnology and Oceanography*, **17**, 327–340.

Sheldon R. W., W. H. Sutcliff and M. A. Paranjape (1977) Structure of pelagic food chain and relationship between plankton and fish production. *Journal of the Fisheries Research Board of Canada*, **34**, 2344–2353.

Sprules W. G. and M. Munawar (1986) Plankton size spectra in relation to ecosystem productivity, size, and perturbation. *Canadian Journal of Fisheries and Aquatic Science*, **43**, 1789–1794.

Wiebe P. H. (1970) Small-scale spatial distribution in oceanic zooplankton. *Limnology and Oceanography*, **14**, 205–217.

Wiebe P. H., A. W. Morton, A. M. Bradley, R. H. Backus, J. E. Craddock, V. Barber, T. J. Cowles and G. R. Flierl (1987) New developments in the MOCNESS, an apparatus for sampling zooplankton and micronekton. *Marine Biology*, **87**, 313–323.